International Journal of Heat and Mass Transfer 71 (2014) 149–157

Contents lists available at ScienceDirect

International Journal of Heat and Mass Transfer

journal homepage: www.elsevier.com/locate/ijhmt

Heterogeneous bubble nucleation on ideally-smooth horizontal heated surface

HangJin Jo [a,b], Massoud Kaviany [a,c], Seol Ha Kim [a], Moo Hwan Kim [a,*]

[a] Division of Advanced Nuclear Engineering, POSTECH, Pohang 790-784, Republic of Korea
[b] Two Phase Flow Laboratory, Institute of Environmental and Energy Technology, Pohang 790-784, Republic of Korea
[c] Department of Mechanical Engineering, University of Michigan, Ann Arbor, MI 48109, USA

ARTICLE INFO

Article history:
Received 14 August 2013
Received in revised form 11 December 2013
Accepted 13 December 2013

Keywords:
Heterogeneous bubble nucleation
Boiling
Modeling
Kinetic dynamics
Thermodynamic stability

ABSTRACT

Our experiments and analyses of the bubble incipient on ideally-smooth, horizontal heated surface confirm the observed low superheat and the weak surface-wettability dependence. These are contrary to the previous heterogeneous nucleation predictions, so to clarify this difference and the experimental results not explained by previous nucleation theories we adapt a new model based the thermal boundary layer. The model includes the kinetic dynamics of the superheated liquid and the thermodynamic stability of the generated vapors. The fluid particle transfer rate is estimated with the Smoluchowski equation. Consequently, the incipient bubble nucleation on the ideally-smooth horizontal surface, with different wettability, is described and the predictions match the experiments fairly well.

1. Introduction

The early stages of nucleation theory, referred to as classic nucleation theory (CNT), are based on the Gibbs theory of new phase formation, ideal gas kinetics, and the energy barrier required for nucleus generation [1–5]. The energy barrier is mainly determined by the energy required for generating the new interface and the energy consumed by the phase change of the metastable initial phase to a stable state. In other way, kinetic nucleation theory (KNT) was also developed as a theoretical nucleation theory [6–12]. The main difference between CNT and KNT is how the model calculates the evaporation rate and condensation rate. In CNT, the nucleation rate is derived from the evaporation and condensation rates with an equilibrium distribution. In KNT, however, instead of using the equilibrium distribution, the evaporation and condensation fluxes and their corresponding transfer rates are calculated separately by considering kinetics and the potential field as a driving source. In recent studies, the rate of nucleation in the KNT model was characterized by the mean first passage time by solving the Smoluchowski equation [9–12]. According to previous nucleation theories, saturated water under atmospheric conditions could produce a newly generated bubble at ~300 °C.

The heterogeneous bubble nucleation occurs under transient or steady heating. In transient experiments the classical homogeneous high-superheat limit is observed, since the associated high heating rates prevent growth of vapor bubbles from the surface imperfections [13]. Steady-state results show reduced superheat, since (a) the surface is rarely smooth at the scale of the critical nucleus, and (b) the surface energy heterogeneities such as local hydrophobicity. Corty and Foust [14] and Bankoff [15] suggested that the widely accepted trapped-vapor theory, which states that cavities on commercial heating surfaces can trap vapors and then it act as nuclei, is the most likely theory for explaining the origin of a boiling bubble. In other words, if the surface cavity is larger than the critical nucleus, the cavity traps vapor and becoming nucleus for heterogeneous nucleation at low superheat. Furthermore, the local surface hydrophobicity also induces heterogeneous nucleation at a reduced superheat, since the nanobubbles existing on the hydrophobic sites become activated and form nucleus seed [16,17]. Qi and Klausner [18] hypothesized the occurrence of nanobubbles for heterogeneous nucleation and Nam and Ju [19] analyzed the incipience of nanobubbles at low superheat on Teflon patterned surface. However, the presence of the nanobubbles could be detached via degassing procedure [20]. Thus, there is a continuing debate on the mechanism of bubble nucleation on a hydrophobic surface without surface cavities at low superheat.

Recently, studies regarding bubble nucleation have entered a new phase with the introduction of advanced surface treatment techniques. The most interesting experimental result is heterogeneous boiling bubble nucleation at low superheats (with a superheat for bubble inception of only ~10 K under atmospheric

* Corresponding author. Tel.: +82 54 279 2165; fax: +82 54 279 3199.
E-mail address: mhkim@postech.ac.kr (M.H. Kim).

0017-9310/$ - see front matter © 2013 Elsevier Ltd. All rights reserved.
http://dx.doi.org/10.1016/j.ijheatmasstransfer.2013.12.040

Nomenclature

c	concentration of particles in one dimension (m^{-1})
D	diffusivity ($m^2\ s^{-1}$)
f	distribution function (–)
Gr	Grashof number (–)
g	acceleration of gravity [9.81 ($m\ s^{-2}$)]
h	latent heat ($J\ kg^{-1}$)
J	transfer rate ($s\ m^3$)$^{-1}$
k_B	Boltzmann constant ($J\ K^{-1}$)
L	the length from edge to center of heating surface (m)
n_B	number density of embryos (m^{-3})
P	pressure ($N\ m^{-2}$)
Pr	Prandtl number (–)
Q	survival probability (–)
R_{ideal}	ideal gas constant [8.314 ($J\ (K\ mol)^{-1}$)]
r	radius of nucleus (m)
s	entropy ($J\ (K\ kg)^{-1}$)
T	temperature (K)
t	time (s)
u	internal energy ($J\ kg^{-1}$)
$\vec{u}, \vec{v}$	x- and y-component velocities ($m\ s^{-1}$)
v	specific volume ($m^3\ kg^{-1}$)
x	horizontal position
y	vertical position

Greek symbols

β	volumetric thermal expansion coefficient (K^{-1})
θ	contact angle (°)
δ_t	thermal boundary layer (m)
Φ	dimensionless temperature (–)
φ	potential free energy ($J\ kg^{-1}$)
η	similarity variable (–)
μ	dynamic viscosity ($kg\ (m\ s)^{-1}$)
ρ	density ($kg\ m^{-3}$)
σ	surface tension (N/m)
τ	passage time (s kg)
υ	kinematic viscosity ($m^2\ s^{-1}$)
ψ	stream function (–)

Subscripts

av	average
B	domain B
lv	interface between liquid and vapor phase
sat	saturated state
top	the top of bubble
y	vertical coordinate
0	initial state
∞	bulk state

water-saturated conditions) on a smooth hydrophilic surface that does not have any microstructures to trap a vapor as the seed for the bubble nucleus [21–25]. Using microelectromechanical system (MEMS) techniques for sub-nanometer roughness heating surfaces, researchers have confirmed the phenomenon on a variety of surfaces. Furthermore, researchers report, heterogeneous nucleation at low superheat on hydrophilic nanostructured heated surface, with no microstructure or hydrophobicity to trap vapor for the bubble nucleation [25–28]. These results are contradictory to those predicted by the heterogeneous nucleation theories.

In this study, we explain recent observations of heterogeneous nucleation at reduced superheat on horizontal heated surface free from trapped vapor and under steady-state condition. These contrast the heterogeneous nucleation theories and to clarify this we use a model based on the thermal boundary layer. This combined with the kinetics and dynamics of the superheated liquid and the thermodynamic stability of the generated vapor, leads to prediction of heterogeneous nucleation condition in absence of micro cavities. This model can also be used for hydrophobic heating surfaces.

2. Experiments

To verify the reported nucleation phenomena without surface cavities and at low superheats, we conducted pool boiling experiments with distilled water under atmospheric saturated condition. The electric Joule heating method was employed, using a power supply. The main pool was an aluminum bath and was maintained at a saturated condition by a PID temperature controller. A thin-film (platinum) heater was embedded on one side of the silicon wafer, and smooth surfaces were fabricated on the other side of the wafer via micro-electromechanical system techniques. The complete platinum film heater was H-shaped due to the configuration of the electrode and the main heating components. The central region of the H-shape (10×10 mm) was the main heating area. Based on the measured resistance of heater and the correlation developed between resistance and wall temperature, the wall temperature was determined. Taking all instrument errors into account, the maximum uncertainty in the wall superheat is less than 1.2 °C over the measured range of the ONB [24,25].

To analyze the heterogeneous nucleation temperature for different wetting surfaces, we used two different wetting smooth surfaces: silicon and heptadecafluoro-1,1,2,2-tetrahydrodecyltrichlorosilane (HDFS) coated surface. The plain silicon wafer possesses a very smooth surface with sub-nanometer surface roughness. The HDFS was coated on silicon surface as a very thin layer using self-assembled monolayer (SAM) technique. As Fig. 1 shows, the plain silicon had a 72° static contact angle, while the static contact angle was 106° for the HDFS coated silicon surface.

To avoid the effect of trapped vapors on the surface cavity, the roughness of each surface should be smaller than the critical radius of the nucleus. The critical radius of the newly generated nucleus can be obtained by differentiating the energy barrier equation based on the Gibbs–Duhem equation (because there exists a maximum energy barrier for the nucleus at the critical condition), i.e.,

$$r_c = \frac{2\sigma_{lv}}{P_{sat}(T_l)\exp\left[\frac{\upsilon_l(P_l - P_{sat}(T_l))}{R_{ideal}T_l}\right] - P_l}. \quad (1)$$

According to the result, the critical radius of the nucleus is of the order of 1 μm (Fig. 2). However, the measured roughness of all surfaces were in the nanometer range, as shown in Table 1. This supports that the roughness of these surfaces could not trap vapor as the seed for the nucleation.

All experiments were conducted after degassing procedure for 2 h. With the system open to ambient air pressure through the reflux condenser, the degassed air was expelled while the steam condensed and returned back to the vessel. The tests were carried out by increasing the electrical input in small steps, until the ONB was reached.

Repeatable results for each surface were obtained up and including the ONB. The required superheats for the silicon and HDFS coated surface at the ONB were 10.7 and 4.4 K, respectively.

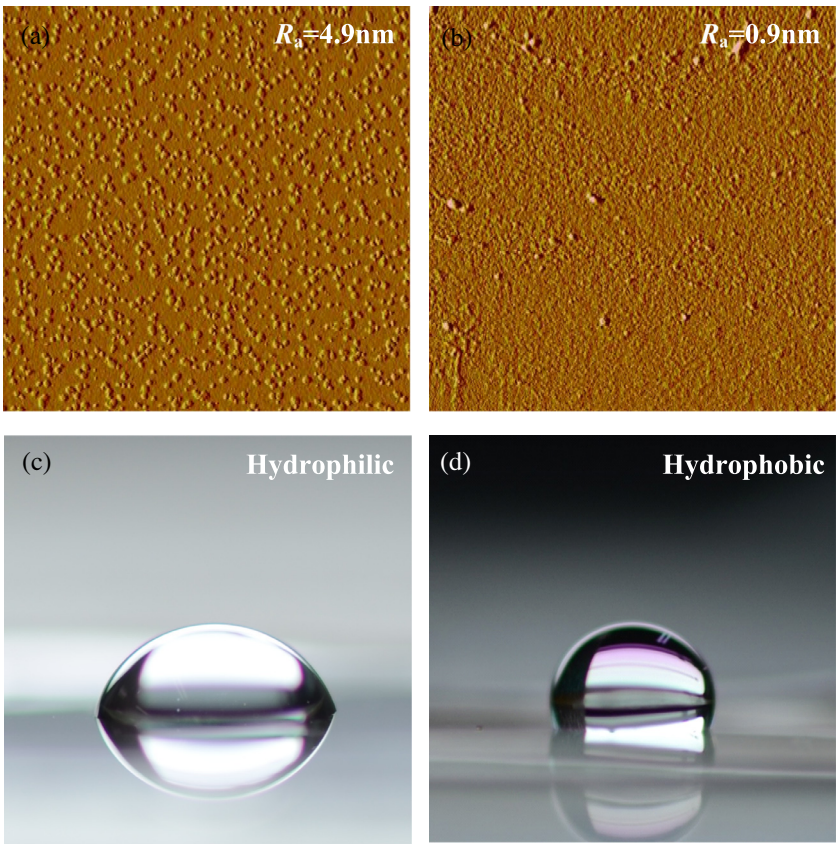

Fig. 1. The heated surfaces used in experiments: (a) AFM image of the silicon surface, and (b) HDFS coated surface. Both actual areas are 5 × 5μm. (c) A 3 μl water droplet and its contact angle on the silicon surface (as a hydrophilic surface), and (d) HDFS coated surface coated surface (as a hydrophobic surface). The roughness statistics and contact angles are listed in Table 1.

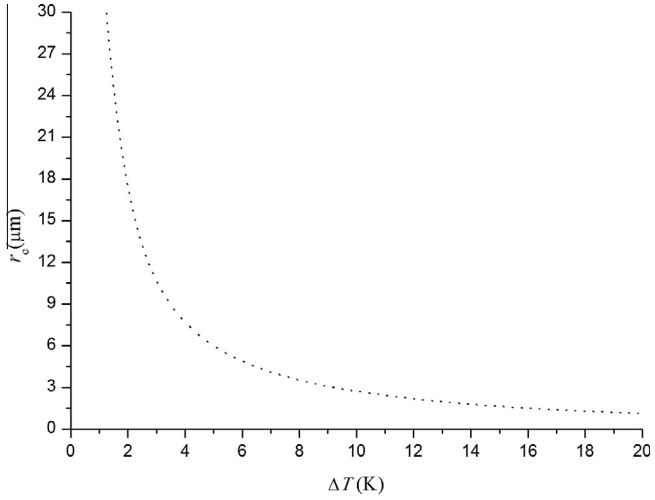

Fig. 2. Dependence of the critical radius of distilled water on wall temperature for atmospheric saturated water.

Table 1
Roughness parameters and water contact angle for the silicon and HDFS coated surfaces used this study. Roughness parameters were measured by AFM.

	R_a (nm)	R_q (nm)	R_{max} (nm)	Contact angle (°)
Silicon	4.9	6.6	50.8	72
HDFS coated	0.9	1.9	51.7	106

The most important observation is that the ONBs for all smooth heating surfaces were definitely lower than the predicted values (280–300 °C) by the classic heterogeneous nucleation models without surface cavities, whether the heating surface was hydrophilic or hydrophobic. This is consistent with the previously reported results for several smooth and nanostructured surfaces [21–28].

3. Theory

To theoretically investigate the heterogeneous bubble nucleation without cavities, we use the potential gradient in the thermal boundary layer adjacent to heated surface for an ideally smooth heated surface. An ideal smooth heated surface has defects that are smaller than the critical size required for the stability of vapor existence on the heated surface; i.e., the vapor cannot be trapped on the surface. The total potential of the system is dependent on the temperature and pressure conditions, which can be represented as the Gibbs free energy:

$$d\phi = du + Pdv + vdP - Tds - sdT. \quad (2)$$

In previous models, the internal energy, volume, pressure, entropy, and temperature difference were not considered for nucleation, because the supplied heat effect and induced flow in the fluid phase were not adopted. However, in real boiling on heated surfaces, there is a definite temperature distribution, due to the supplied heat through the heated surface, as well as a pressure difference (represented by the vertical flow rate) on the heated surface. In this study, for describing the real potential distribution adjacent to the heated surface, the temperature and pressure of the fluid at or just before boiling bubble nucleation are evaluated using similarity analysis for natural convection on a horizontal flat hot surface, with an approximated thermal boundary layer thickness [29,30].

3.1. Evaluating potential gradient on a horizontal heating surface

To evaluate the potential gradient, for thermobuoyant flow over semi-infinite horizontal surface, the temperature and pressure distributions are evaluated. The continuity, momentum, and energy equation are expressed by the Boussinesq relation, under two-dimensional, boundary-layer approximations (x and y are for horizontal and vertical axes) are

$$\frac{\partial \vec{u}}{\partial x}+\frac{\partial \vec{v}}{\partial y}=0 \tag{3}$$

$$\vec{u}\frac{\partial \vec{u}}{\partial x}+\vec{v}\frac{\partial \vec{u}}{\partial y}=-\frac{1}{\rho}\frac{\partial P}{\partial x}+\vec{v}\frac{\partial^2 \vec{u}}{\partial y^2} \tag{4}$$

$$0=-\frac{1}{\rho}\frac{\partial P}{\partial y}+g\beta(T-T_\infty) \tag{5}$$

$$\vec{u}\frac{\partial T}{\partial x}+\vec{v}\frac{\partial T}{\partial y}=\alpha\frac{\partial^2 T}{\partial y^2}. \tag{6}$$

It should be noted that P used in these governing equations is the dynamic pressure difference induced by the buoyancy force. The governing equations are reduced using the Grashof number and a similarity variable $\eta(x,y)$

$$Gr_x=\frac{g\beta(\Delta T)x^3}{\nu^2}. \tag{7}$$

$$\eta(x,y)=\frac{y}{x}\left(\frac{Gr}{5}\right)^{1/5}=\frac{y}{x}\left(\frac{g\beta(\Delta T)x^3}{5\nu^2}\right)^{1/5}=\left(\frac{g\beta(\Delta T)}{5\nu^2}\right)^{1/5}yx^{-2/5}. \tag{8}$$

Based on this variable, the stream function ψ and dimensionless temperature are defined as

$$\psi(x,y)=\frac{y}{x}\left(\frac{Gr}{5}\right)^{1/5}f(\eta)=\frac{y}{x}\left(\frac{g\beta(\Delta T)x^3}{5\nu^2}\right)^{1/5}f(\eta). \tag{9}$$

$$T^*(x,y)=\frac{T-T_\infty}{\Delta T}=\Phi(\eta). \tag{10}$$

Owing to the temperature distribution along the heating surface, ΔT could change with the heating surface and liquid condition. Therefore, ΔT is assumed with some positive constant N depending on x as Nx^n ($\Delta T = Nx^n$). The constant for presenting the temperature variation (n) along the x direction is fixed as 1/3 for the constant heat flux condition [29]. If the center temperature is known, N could be represented with the length from the center to the end of heating surface as

$$N=\frac{\Delta T_{x=L}}{L^n}. \tag{11}$$

$$\Delta T=\Delta T_{x=L}\left(\frac{x}{L}\right)^n. \tag{12}$$

where L denotes the length from edge to center of heating surface. In here, L will be 5 mm.

Chen et al. [29] and Pera and Gebhart [30] presented numerical simulation results for the temperature profile on a horizontal hot surface using governing equations and similarity variables. Evaluating the exact solution for the temperature and pressure profiles with natural convection flow is difficult. However, the complicated profile could be approximated as the proper functional expression with constrained boundary conditions in the thin range adjacent to the heating surface. In this study, the thin region is related to the critical size of nucleation. ($1 \gg \eta$)

Based on reported numerical simulation results, the trend lines of the general dimensionless temperature profile in the thermal boundary layer on a horizontal heating layer could be approximated to the exponential function ['$a\exp(-b\eta)$'] as shown in Fig. 3 (a and b are arbitrary constants for the given system). Although the arbitrary constants depend on other parameters, the form of the general function is kept. Therefore, we adopt the exponential function as the approximated dimensionless temperature profile in the thermal boundary layer:

$$T^*(x,y)=a\exp(-b\eta)=a\exp\left(-b\left(\frac{g\beta\Delta T_{x=L}}{5\nu^2L^n}\right)^{1/5}yx^{(n-2)/5}\right). \tag{13}$$

$$T^*(x,0)=1,\quad T^*(x,1)=0\quad\text{and}\quad T^*(x,\delta_t)=0.01.\qquad\text{Boundary condition of } T^* \tag{14}$$

Because of the initial condition, the constant a is determined to be unity. Among the boundary conditions, $T^*(x,\delta_t)=0.01$ arises from the definition of the thermal boundary layer. Let the thickness of the thermal boundary at the center of the heater surface be $\delta_{t_{x=L}}$. With the boundary conditions and the distance from the edge to the center of the heating surface (L) [$T^*(L,0)=1$ and $T^*(L,\delta_{t,x=L})=0.01$], the temperature profile is specified as

$$0.01=\exp\left(-b\left(\frac{g\beta\Delta T_{x=L}}{5\nu^2L^n}\right)^{1/5}\delta_{t,x=L}L^{(n-2)/5}\right). \tag{15}$$

$$b=\frac{(\ln 100)}{\left(\frac{g\beta\Delta T_{x=L}}{5\nu^2L^n}\right)^{1/5}\delta_{t,x=L}L^{(n-2)/5}}. \tag{16}$$

Substituting equation Eq. (17) into Eq. (13), one obtains the following dimensionless temperature profile

$$T^*(x,y)=\frac{T-T_\infty}{T_0-T_\infty}=\exp\left(-\frac{\ln 100}{\delta_{t,x=L}}y\left(\frac{x}{L}\right)^{(n-2)/5}\right). \tag{17}$$

Eq. (18) is the approximated solution in a certain domain from the surface to δ_t by analyzing the trend line of the numerical solution for natural convection on a horizontal heating surface. However, even though the equation is not theoretically derived, the accuracy of the calculated temperature profile will be high near the boundary condition because the accuracy is calibrated by the boundary condition at zero and δ_t height (c.f. $\delta_{t,x=L}$ is approximated to be 210 μm based on the pool boiling experimental results with Fourier's law $\delta_t = k\frac{T-T_w}{q''}$; this is similar to value (100 μm) used in

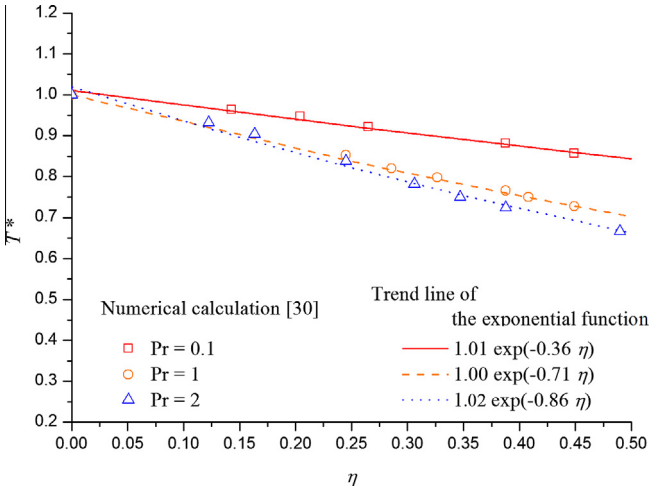

Fig. 3. Dimensionless temperature distributions from the numerical simulations [30], and from the trend-line approximated by the exponential function.

other classic literature for water boiling systems [31].). Furthermore, the domain of interest for nucleation is very small, and the evaluated solution, Eq. (18), could be reasonably applied to the nucleation phenomena. The dynamic pressure was estimated by the relation between the pressure function and the dimensionless temperature [29,30].

Finally, the potential gradient distribution of the superheated liquid on the horizontal heating surface could be investigated by incorporating the temperature profile with the appropriate boundary conditions and the pressure profile. (Although the temperature profile is approximated to the exponential function, because the interesting domain is very thin, we can see the linear trend in Fig. 4.)

3.2. Superheated liquid particles transfer in potential gradient

The evaluated potential profile on the horizontal heated surface is represented using the Smoluchowski's equation to obtain an appropriate fluid particle transfer rate on the ideal smooth horizontal heated surface. In general, the physical random motion of molecules is governed by the Fokker–Planck equation [32,33]. However, because the relaxation time for the velocity distribution is extremely short and negligible, the Fokker–Planck equation for a liquid can be reduced to the Smoluchowski equation. The Smoluchowski equation, with diffusion and convection terms, can be expressed as

$$\frac{\partial c}{\partial t} = \nabla \cdot (D\nabla c - vc) \cong \nabla \cdot \left(-\frac{D}{k_B T}\nabla \phi c\right), \tag{18}$$

where c indicates the particle concentration (or the probability of a molecule being in a certain region at time t). The movement of particles in the thermal boundary layer can be expressed by substituting the evaluated potential distribution of the horizontal heated surface for the convection mass-flux term in Eq. (18). In this study, we assume that the convection mass-flux term is dominant. This approximation is reasonable for the potential gradient model, because there is the macroscopic flow induced by the temperature distribution and density difference; the diffusion term on the right-hand side of Eq. (18) is negligible.

With the evaluated potential profile and the Smoluchowski equation, the mean first-passage time is estimated for characterizing the nucleation rate on the horizontal heated surface. The mean first-passage time for boiling specifies the average time required for the particles of the working fluid to move from the certain bubble region to the outside. By setting the calculation domain (domain B) to be the critical state of newly generated nuclei, the mean first-passage time could represent the evaporation rate of real boiling on the horizontal heated surface as shown in Fig. 5.

To determine the mean first-passage time, the survival probability $Q(t)$, i.e., how many molecules will remain in the domain after time t, is defined as

$$Q(t|y_o) = \int^B c(y,t|y_o)dy \quad \text{Survival probability in domain B after time } t \tag{19-a}$$

$$Q(t\to\infty|y_o) = 0 \quad \text{and} \quad Q(t=0|y_o) = 1 \quad \text{Initial conditions of } Q. \tag{19-b}$$

The initial conditions of survival probability indicate that all of the molecules initially located in the domain will escape from the domain after an infinite time by molecule transfer dynamics. The survival probability can be transformed to the probability of escaping from the domain as $1 - Q(t)$. The mean first-passage time is expressed by the mean average of the survival probability integrated with respect to time as

$$\tau(y_o) = \int_0^\infty t dt \frac{\partial}{\partial t}[1 - Q(t|y_o)] = \int_0^\infty dt \cdot Q(t|y_o). \tag{20}$$

If Eq. (18) is integrated with respect to position y over the domain from time $t = 0$ to ∞, then we obtain

$$\int_0^\infty \int^B \frac{\partial c}{\partial t} dy dt = \int_0^\infty \int^B \nabla \cdot \left(-\frac{D}{k_B T}\nabla \phi c\right) dy dt. \tag{21}$$

Integrating with respect to y transforms the probability of the molecules being in a certain bubble region at time t into the survival probability, Q, in the domain:

$$\int_0^\infty \frac{\partial Q(t|y_o)}{\partial t} dt = \int_0^\infty \nabla \cdot \left[-\frac{D}{k_B T}\nabla \phi Q(t|y_o)\right] dt. \tag{22}$$

The survival probability can be described in terms of the mean average of the escape probability by the initial condition of Q (Eq. (19-b)):

$$\tau(y_o) = \int_0^{y_o} 1 \Big/ \left(\frac{D}{k_B T}\nabla \phi\right) dy. \tag{23}$$

The escape time, τ, of a certain domain can be developed with the evaluated potential distribution on the horizontal heated surface in the thermal boundary layer, given by Eq. (2), and the Stokes–Einstein equation for the diffusivity:

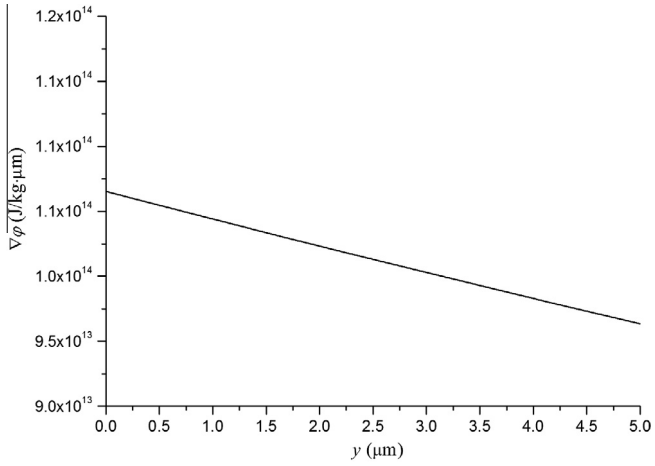

Fig. 4. Potential gradient distributions along the vertical direction, at the center of heated region ($\theta = 60°$, $\Delta T = 5$ K and $\delta_t = 210$ μm).

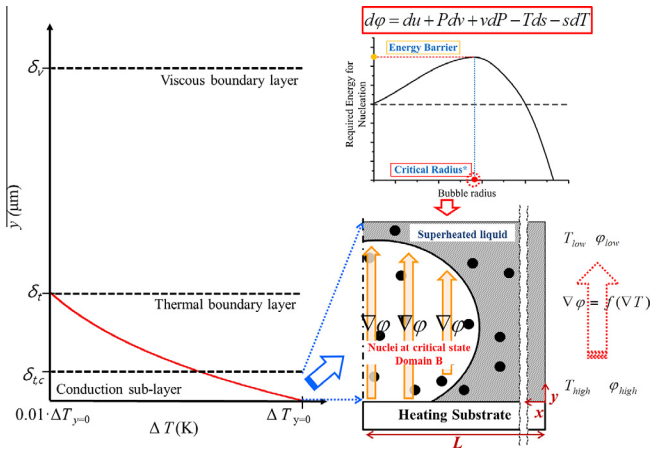

Fig. 5. Schematics of the temperature distribution, thermal boundary layer, total energy as function of bubble radius, and the bubble nucleation.

$$\tau(y_o) = \int_0^{y_o} 1 \Big/ \left[\frac{1}{6\pi\mu r_o}\left(\frac{\partial u}{\partial y} + P\frac{\partial v}{\partial y} + v\frac{\partial P}{\partial y} - T\frac{\partial s}{\partial y} - s\frac{\partial T}{\partial y}\right)\right] dy. \tag{24}$$

where r_o is the radius of fluid particle. The final average escape time for all possible initial positions in the domain, weighted by the Boltzmann factor with an equilibrium distribution of particles (or molecules), is given by

$$\tau_{av} = \frac{\int^B \tau(y_o)\exp\left(\frac{-\Delta\phi}{k_B T}\right)dy}{\int^B \exp\left(\frac{-\Delta\phi}{k_B T}\right)dy}. \tag{25}$$

Consequently, the transfer rate of superheated liquid particles in the domain can be defined by n, the number of molecules in the domain, as

$$J = \rho\frac{n_B}{\tau_{av}}. \tag{26}$$

To include the spatial variation of transfer rates, each calculated flux is averaged for the bubble regime. For the averaging procedure, the bubble domain from the center of the nucleus to the end of the bubble nucleus was divided into 100 small sections. Then, the transfer rate was estimated with the number of particles and the average escape time along the y axes at each position. Finally, by normalizing the sum of the transfer rate at each local position by the number of divided sections (100), the average transfer rate of the nucleus (J_{av}) can be obtained.

Figs. 6 and 7 show the evaluated each evaporation rate for each small sections and average evaporation rate for the domain on the horizontal heated surface. These results are calculated for atmospheric saturated water boiling with superheated surfaces. Basically, in the calculation thermal boundary layer was assumed as 210 μm based on experimental results. However, because we could not know the exact thickness of thermal boundary layer, we calculated average evaporation rates for different thickness cases. According to the results, we can confirm very high transfer rates in the 10^2 μm order of thermal boundary thickness. It indicates that the liquid particles in the potential gradient (the thermal boundary layer) move out with a very high transfer rate from the domain to the outside, where the potential is lower than that in the previous location, even though the exact transfer rate is slightly dependent on the surface characteristics and the superheated condition.

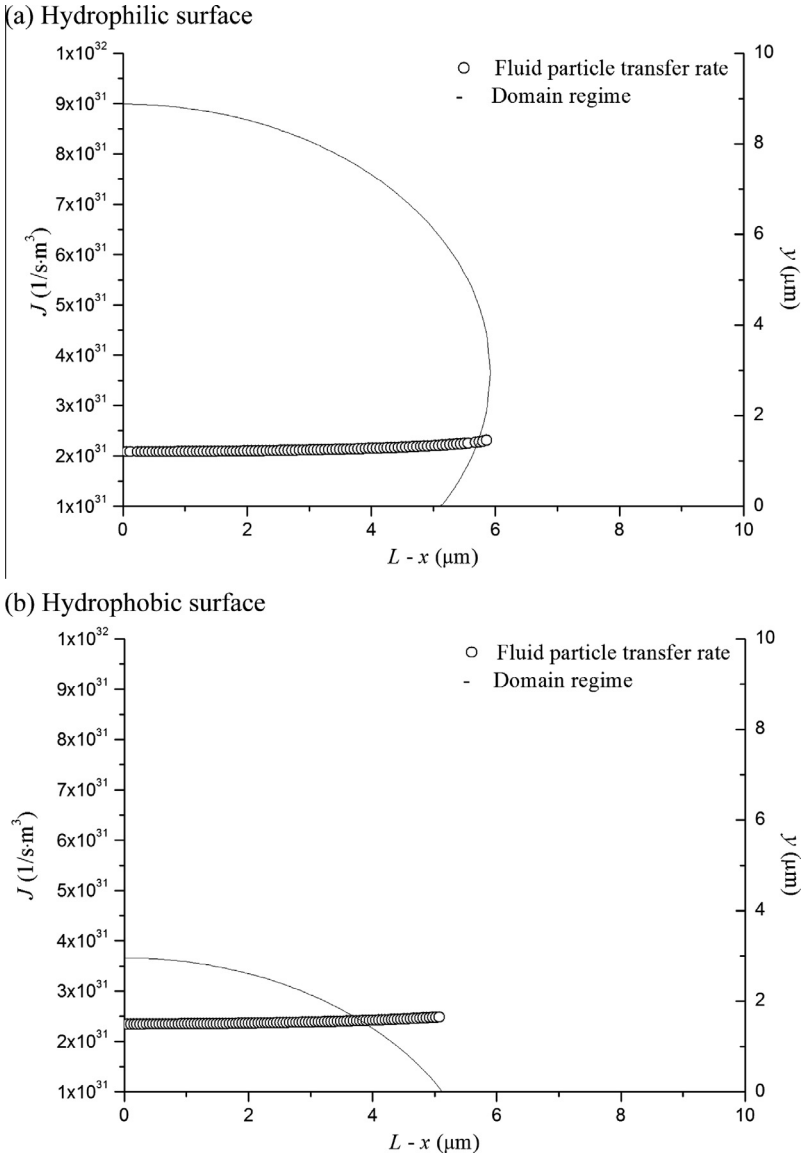

Fig. 6. Lateral distribution of the fluid particle transfer rate and bubble contour for, (a) $\theta = 60°$, and (b) $\theta = 120°$, for the critical nucleus condition and $\Delta T = 5$ K under atmospheric saturated water condition. $L - x = 0$ is at the center of surface.

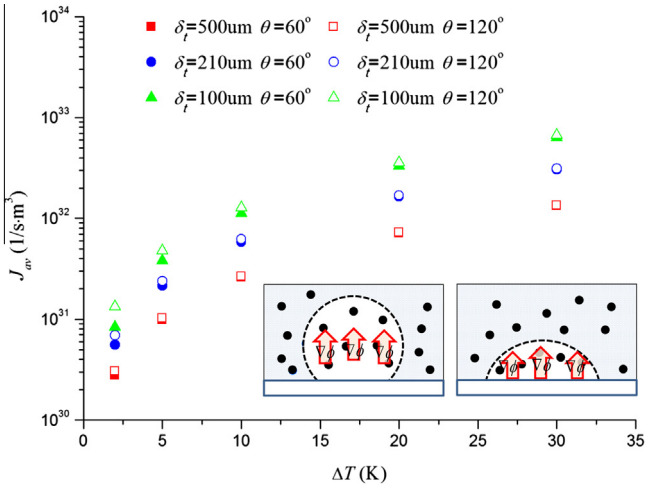

Fig. 7. Variations of the average fluid particle transfer rate for critical nucleus formation as function of wall superheat for two different contact angles under atmospheric saturated water condition with different thermal boundary layer thicknesses.

By such high liquid molecules transfer rate, a spontaneous decrease in the number of particles in the domain occurs, which may promote the initiation of bubble generation, because to initiate a phase change from liquid to vapor, a large density decrease is required. Interestingly, the order of evaluated nucleation rates is as high as the calculated nucleation rates for the moment of heterogeneous nucleation using PFT (phase field theory) [34] and MD (molecular dynamics) simulation tool [35]. This supports that the calculated transfer rate for the new nuclei is sufficiently high to lead to ebullition. From this, we can conclude that the induced potential gradient on the ideally smooth horizontal heated surface, due to the supplied heat, causes large enough particle transfer to generate vapor.

Such high transfer rates of liquid particles adjacent to the heated surface are directly related to energy gradient in the thermal boundary layer. To clarify the thermal boundary layer effect, we also calculated what would happen if the thermal boundary layer was very thin compared with the critical nucleus (calculation domain B). When the thermal boundary layer is very thin compared with the critical nucleus, we can neglect the effect of potential gradient, such as previous nucleation models. The critical nucleus is 2.7 μm for water at $T = 110$ °C. So a submicron thermal boundary layer thickness of 0.21 μm is assumed here to investigate the fluid particle transfer rate with negligible potential gradient, to investigate the superheat for incipient heterogeneous nucleation. With this boundary layer thickness (1000 × smaller than the thickness used in previous studies), the transfer rate is nearly uniform and approximately 10^{-35} (m^3 s)$^{-1}$. Such a low transfer rate with a very thin thermal boundary condition could not induce bubble nucleation and it corresponds well with the classic nucleation predictions that were derived without the potential gradient. It implies that the representation of bubble nucleation discussed in this study is compatible with the results of previous classical nucleation models.

3.3. Thermo dynamical equilibrium for nucleation

We confirm the high evaporation rates of fluid particle in the potential gradient on the heated horizontal surface by considering the kinetic motion of fluid particle. However, although there are very high transfer rates of fluid particle, the imbalance of particle transfer for the domain cannot be maintained for long if the domain is not in an equilibrium state for a new bubble at the same time. So, we also consider the thermo-equilibrium state of the generated bubble by the high evaporation rate for determining the condition of bubble nucleation. The equilibrium condition is determined by comparing the required temperature of the vapor for equilibrium with the surrounding liquid temperature at the top of the bubble. The temperature profile of working fluid is calculated from the similarity analysis for natural convection on a horizontal flat hot surface, as mentioned before. The required superheat of the vapor for equilibrium is evaluated by the Clausius–Clapeyron equation. If the environmental temperature is lower than the required temperature for equilibrium, the generated vapor will disappear for an instant. Therefore, the criterion for thermal stability of the vapor clusters is given as

$$\Delta T_{top} \geqslant \left(\frac{T_{sat}}{h_{lv}} v_{lv} \Delta P\right). \tag{27}$$

where ΔT_{top} is the superheat of working fluid at the top of bubble. v_{lv} and ΔP indicate the volume and pressure change of the phase transition, respectively. For comparison, the thermo stability is determined by dividing the superheat of working fluid at the top of bubble by the required superheat for equilibrium, $\Delta T_{top} / \left(\frac{T_{sat}}{h_{lv}} v_{lv} \Delta P\right)$. (Owing to the variation of the height of the formed vapor, the temperature required for stability is dependent on the wettability of the surface as shown in Fig. 8.) We already confirm that the kinetic transfer rates of fluid particle are sufficiently high to promote bubble nucleation in the potential gradient on the horizontal heated surface. It indicates that the bubble initiation condition could be predicted when the thermo-equilibrium of the generated bubble is satisfied. Consequently, if the normalized equilibrium parameter is larger than or equal 1 with the high evaporation rate, the bubble could be nucleated.

Fig. 9(a) and (b) show the thermal stability and the predicted bubble nucleation region for several wetting surfaces. As shown in Fig. 9(a), the heterogeneous bubble nucleation is predicted over 9 K superheat for any smooth heating surfaces when the thickness of thermal boundary layer is 210 μm. Even if the thermal boundary layer thickness is 100 μm, the heterogeneous bubble could be nucleated below the superheat of 13 K.

Fig. 9(b) shows the result of comparison with experimental data with smooth heating surface conducted in this study and previous reports. The theoretically predicted superheats for bubble nucleation within 210 μm thermal boundary layer are 5.3 K for a heating

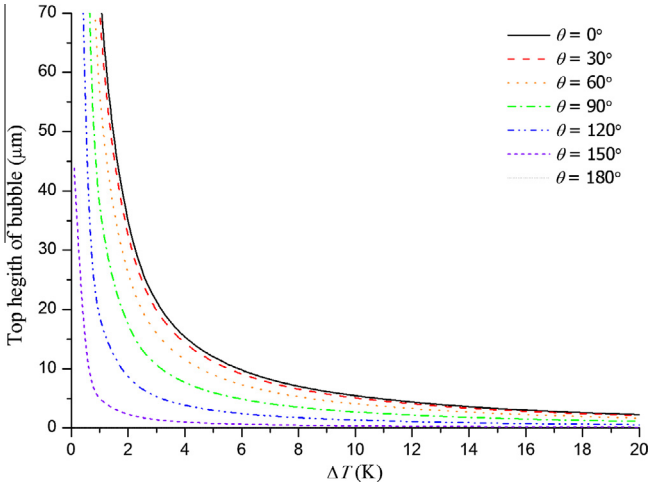

Fig. 8. The height of virtual bubble at the critical condition for nucleation on different wettability characteristics under atmospheric saturated condition.

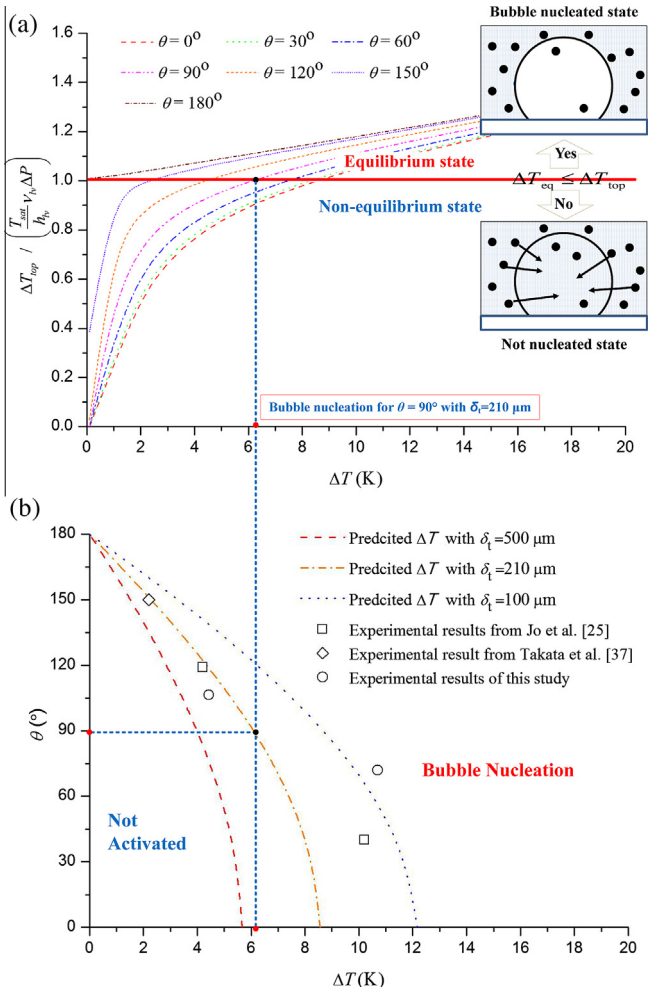

Fig. 9. (a) Required superheat for the thermal stability for various contact angles (δ_t = 210 μm) and (b) comparison of predicted superheats as a function of contact angle for different thermal boundary layer thicknesses with experiments. The results are for atmospheric saturated water condition.

surface with a 106° contact angle and 7 K for 72° contact angle heating surface. In this study, experimentally reported ONBs for hydrophobic (θ = 106°) and hydrophilic (θ = 72°) surfaces are 4.4 and 10.7 K, respectively. The predicted superheat for nucleation varies from 4.4 to 8.1 K; the contact angles ranges from 120° to 40°. These results are in good agreement with the experimental results of Jo et al., whose study showed that on a Teflon-coated surface and a oxidized silicon surface, the first bubble was observed at 4.2 and 10.2 K superheat, respectively [25]. For a heated surface with a 150° contact angle, the predicted superheat of new bubble ebullition was 2.3 K. This prediction also agrees well with the experimental results of Takata et al. of 2.2 K [36].

The present model predicts 2–10 K superheats for bubble nucleation without trapped vapor. It is a more precise prediction compared than the previous nucleation models for a smooth heating surface. Furthermore, the model correctly depicts the trend that is increasing superheat for bubble nucleation as the contact angle decreases. Even though the agreement between the data and the model is quite good, the present model will be extended for other working fluids as further research.

4. Conclusions

To better understand bubble nucleation on smooth surfaces with different wettabilities, experimental and theoretical investigations are conducted. In our nucleation model, the potential gradient is used to describe the bubble nucleation, adopting the kinetics of superheated liquid within thermal boundary layer and the thermodynamic stability of the generated vapor. The evaporation rate in the thermal boundary layer is estimated and as expected it is high in order to activate the nucleation phenomenon. The thermal non-equilibrium of the instantly generated bubble nucleus by this high evaporation rate is also evaluated via comparison of the equilibrium temperature of the generated vapor with the temperature of the surrounding liquid. Consequently, we can predict the bubble nucleation condition under thermal equilibrium of the generated bubble and satisfying the high evaporation rate within the thermal boundary layer. Our analysis of the bubble incipient on ideally-smooth horizontal surfaces, supports the observed low incipient nucleate boiling superheat under different wetting surfaces. The results from this study provide fundamental understanding of the incipient boiling.

Acknowledgments

This work was supported by the National Research Foundation of Korea (NRF) Grant funded by the Korea government (MSIP) (2012R1A2A1A01003376).

References

[1] J.W. Gibbs, The Collected Works, Longmans Green and Company, New York, 1928.
[2] V.P. Carey, Liquid–Vapor Phase-Change Phenomena, Hemisphere Publishing Corporation, United Kingdom, 1992.
[3] Y. Kagan, The kinetics of boiling of a pure liquid, Russ. J. Phys. Chem. 34 (1960) 42–48.
[4] M. Volmer, A. Weber, Keimbildung in übersättigten Gebilden, Z. Phys. Chem. 119 (1926) 277–301.
[5] M. Blander, J.L. Katz, Bubble nucleation in liquids, AIChE J. 21 (1975) 833–848.
[6] J.L. Katz, H. Wiedersich, Nucleation theory without Maxwell demons, J. Colloid Interface Sci. 61 (1977) 351–355.
[7] J.L. Katz, M.D. Donohue, A kinetic approach to homogeneous nucleation theory, Adv. Chem. Phys. 40 (1979) 137–155.
[8] S.L. Girshick, C.P. Chiu, Kinetic nucleation theory: a new expression for the rate of homogeneous nucleation from an ideal supersaturated vapor, J. Chem. Phys. 93 (1990) 1273–1277.
[9] A. Szabo, K. Schulten, Z. Schulten, First passage time approach to diffusion controlled reactions, J. Chem. Phys. 72 (1980) 4350–4357.
[10] V.K. Shen, P.G. Debenedetti, A kinetic theory of homogeneous bubble nucleation, J. Chem. Phys. 118 (2003) 768–783.
[11] E. Ruckenstein, Y.S. Djikaev, Recent developments in the kinetic theory of nucleation, Adv. Colloid Interface Sci. 118 (2005) 51–72.
[12] K.M. Hong, J. Noolandi, Solution of the Smoluchowski equation with a Coulomb potential. I. General results, J. Chem. Phys. 68 (1978) 5163–5169.
[13] S. Glod, D. Poulikakos, Z. Zhao, G. Yadigaroglu, An investigation of microscale explosive vaporization of water on an ultrathin Pt wire, Int. J. Heat Mass Transfer 45 (2002) 367–379.
[14] C. Corty, A.S. Foust, Surface variables in nucleate boiling, Chem. Eng. Prog. Symp. Ser. 51 (1955) 1–12.
[15] S.G. Bankoff, Entrapment of gas in the spreading of a liquid over a rough surface, AIChE J. 4 (1958) 24–26.
[16] J.W.G. Tyrrell, P. Attard, Images of nanobubbles on hydrophobic surfaces and their interactions, Phys. Rev. Lett. 87 (2001) 176104.
[17] S. Yang, S.M. Dammer, N. Bremond, H.J.W. Zandvliet, E.S. Kooij, D. Lohse, Characterization of nanobubbles on hydrophobic surfaces in water, Langmuir 23 (2007) 7072–7077.
[18] Y. Qi, J.F. Klausner, Comparison of nucleation site density for pool boiling and gas nucleation, J. Heat Transfer 128 (2006) 13–20.
[19] Y. Nam, Y.S. Ju, Bubble nucleation on hydrophobic islands provides evidence to anomalously high contact angles of nanobubbles, Appl. Phys. Lett. 93 (2008) 103115.
[20] X.H. Zhang, G. Li, N. Maeda, J. Hu, Removal of induced nanobubbles from water/graphite interfaces by partial degassing, Langmuir 22 (2006) 9238–9243.
[21] H.T. Phan, N. Caney, P. Marty, S. Colasson, J. Gavillet, Surface wettability control by nanocoating: the effects on pool boiling heat transfer and nucleation mechanism, Int. J. Heat Mass Transfer 52 (2009) 5459–5471.
[22] T. Chen, J.F. Klausner, S.V. Garimella, J.N. Chung, Subcooled boiling incipience on a highly smooth microheater, Int. J. Heat Mass Transfer 49 (2006) 4399–4406.

[23] T.G. Theofanous, J.P. Tu, A.T. Dinh, T.N. Dinh, The boiling crisis phenomenon: Part I: nucleation and nucleate boiling heat transfer, Exp. Therm. Fluid Sci. 26 (2002) 775–792.
[24] H.J. Jo, H.S. Ahn, S.H. Kang, M.H. Kim, A study of nucleate boiling heat transfer on hydrophilic, hydrophobic and heterogeneous wetting surfaces, Int. J. Heat Mass Transfer 54 (25) (2011) 5643–5652.
[25] H.J. Jo, S.H. Kim, M.H. Kim, Nucleate boiling performance on nano/microstructures with different wetting surfaces, Nanoscale Res. Lett. 7 (2012) 1–9.
[26] R. Chen, M. Lu, V. Srinivasan, Z. Wang, H.H. Cho, A. Majumdar, Nanowires for enhanced boiling heat transfer, Nano Lett. 9 (2009) 548–553.
[27] T.J. Hendricks, S. Krishnan, C. Choi, C. Chang, B. Paul, Enhancement of pool-boiling heat transfer using nanostructured surfaces on aluminum and copper, Int. J. Heat Mass Transfer 53 (2010) 3357–3365.
[28] C. Li, Z. Wang, P.I. Wang, Y. Peles, N. Koratkar, G.P. Peterson, Nanostructured copper interfaces for enhanced boiling, Small 4 (2008) 1084–1088.
[29] T.S. Chen, H.C. Tien, B.F. Armaly, Natural convection on horizontal, inclined, and vertical plates with variable surface temperature or heat flux, Int. J. Heat Mass Transfer 29 (1986) 1465–1478.
[30] L. Pera, B. Gebhart, Natural convection boundary layer flow over horizontal and slightly inclined surfaces, Int. J. Heat Mass Transfer 16 (1973) 1131–1146.
[31] Y.Y. Hsu, On the size range of active nucleation cavities on a heating surface, J. Heat Transfer (US) 84 (1962) 207–213.
[32] N. Agmon, Residence times in diffusion processes, J. Chem. Phys. 81 (1984) 3644–3647.
[33] C.W. Gardiner, Handbook of Stochastic Methods, Springer, Berlin, 1985.
[34] L. Gránásy, T. Börzsönyi, T. Pusztai, Nucleation and bulk crystallization in binary phase field theory, Phys. Rev. Lett. 88 (2002) 206105.
[35] B.R. Novak, E.J. Maginn, M.J. McCready, Comparison of heterogeneous and homogeneous bubble nucleation using molecular simulations, Phys. Rev. B 75 (2007) 085413.
[36] Y. Takata, S. Hidaka, T. Uraguchi, Boiling feature on a super water-repellent surface, Heat Transfer Eng. 27 (2006) 25–30.